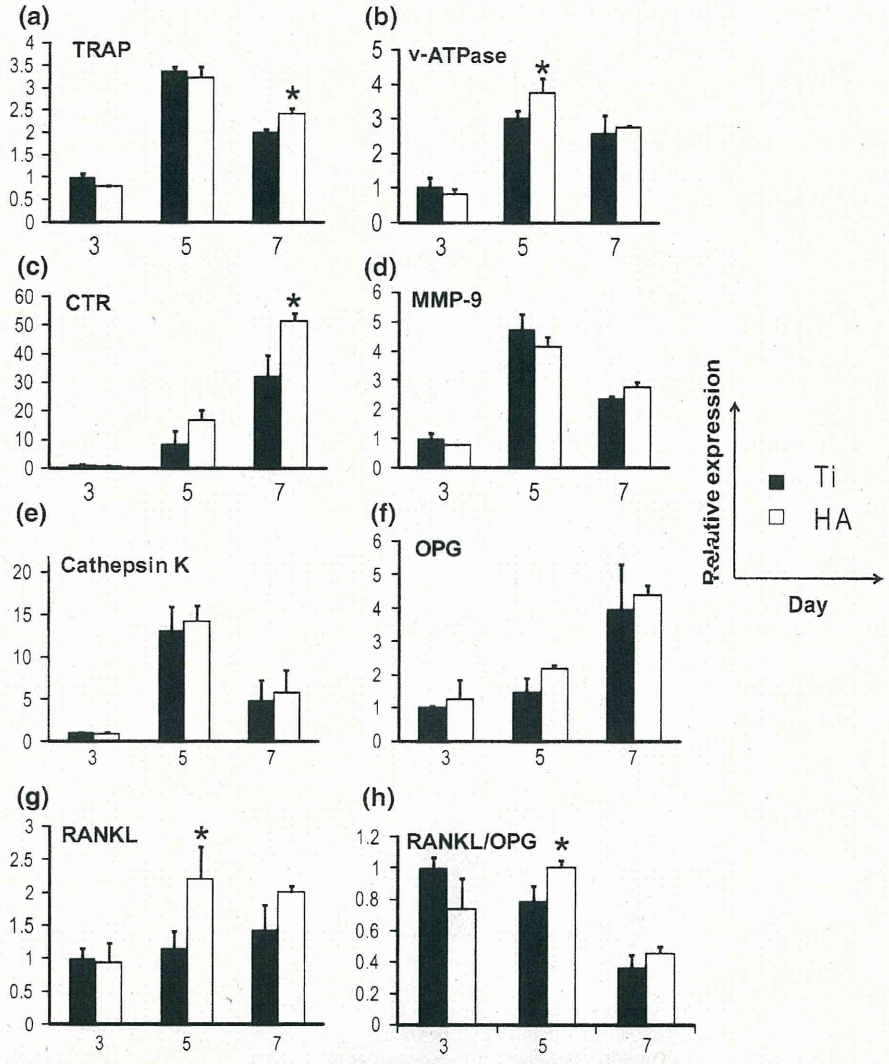

Fig. 6 mRNA expression levels of osteoclast related genes. X-axes represent days of culture, and y-axes represent expression levels relative to Ti group of the first time point. Data are shown as the mean ± SD ($n = 6$). *Statistically different between HA and Ti groups ($P < 0.05$)

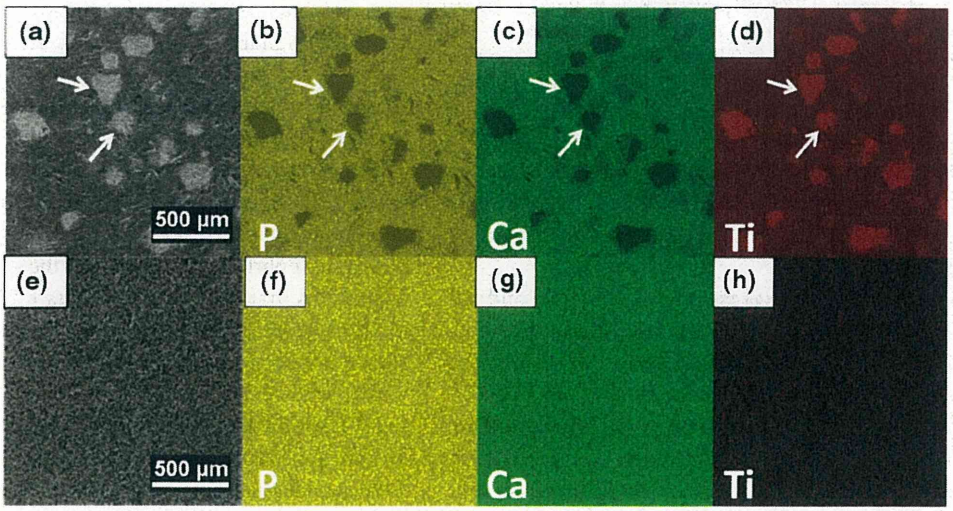

Fig. 7 SEM micrographs of HA coating (**a**, **e**) and corresponding X-ray elemental maps for P in *yellow* (**b**, **f**), Ca in *green* (**c**, **g**) and Ti in *red* (**d**, **h**). Osteoclast culture was performed on the HA coated Ti plates for 7 days and the resorption areas were indicated by *arrows* (**a**–**d**). The HA coated Ti plates with no cells were soaked in the same culture medium for 7 days as control (**e**–**h**)

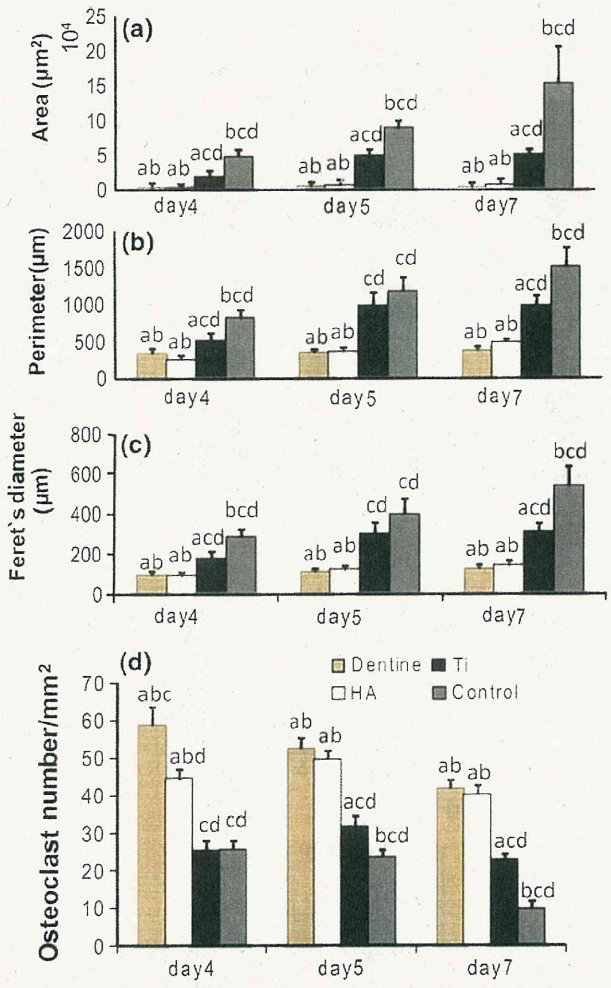

Fig. 5 Osteoclast morphometry. The area (**a**), perimeter (**b**) and Feret's diameter (**c**) (Feret's diameter is the longest distance between any two points along the osteoclast surface) were quantified using an image analyzer (Image J). TRAP positive cells with three or more nuclei were counted (**d**). Each value is represented as the mean ± SD ($n = 6$). Statistically different ($P < 0.01$): **a** compared with control, **b** compared with Ti, **c** compared with HA and **d** compared with dentine

MMP-9 mRNA expression. These results suggest that the sputtered HA surface stimulated osteoclast formation and function by controlling the mRNA transcription that regulates osteoclast.

We also examined the expressions of RANKL and its decoy receptor OPG. The RANKL/OPG ratio plays a crucial role in coordinating the sequence of osteoclast differentiation during the bone remodeling cycle [24]. In the present study, OPG mRNA level was slightly increased on HA than on Ti although the difference was not significant and the level of RANKL mRNA on HA was significantly elevated at day 5, which resulted in an apparent increase in RANKL/OPG ratio favorable for osteoclast formation. A few studies have addressed the effect of implant microtopography on osteoclast formation and activity. Lossdörfer S et al. cultured MG63 cells on titanium disks with different surface roughness, and found that OPG mRNA levels increased on rougher surfaces while RANKL expression was independent of surface microtopography [25]. We observed a higher RANKL/OPG ratio on the sputtered HA than on Ti in the present study. It is probably due to the difference of chemical composition between HA and Ti. Our results for the first time suggested that the sputtered HA surface might stimulate osteoclast formation by up-regulation of RANKL expression from osteoblasts in the co- culture system.

Another explanation of our findings is that HA has the ability to adsorb and release proteins because it has multiple potential protein binding sites and a larger specific surface area compared to other calcium phosphates. The HA film has an adsorption site at the *a*-plane area (Ca^{2+}) and at the *c*-plane area (PO_4^-, OH^-), which can attract acidic proteins with negative sites (COO^-) and basic proteins with positive sites (NH_2^+), respectively [26]. The previous study has reported that the surface area of the sputtered HA film was increased by the hydrothermal treatment, owing to the growth of HA crystals in the *c*-axis direction [27]. The adsorption amount of proteins is proportionate to the surface area of HA, and the release rate of proteins depends on HA resorption [28]. Additionally, osteoclast adhesion and migration are regulated by $\alpha_v\beta_3$ integrin which binds to a variety of extracellular matrix proteins including vitronectin, osteopontin and bone sialoprotein [29], and osteoprogenitor cells and osteoblasts also express a wide panel of integrins, which regulate osteoblast function and mineralization [30, 31]. In the present study, the sputtered HA may promote the osteoblast and osteoclast formation and function through the integrin mediated signaling pathway as a result of recruitment of extracellular matrix proteins onto the coating. Further studies are needed to elucidate the mechanism in detail from this point of view.

Recently, several studies suggested that osteoclast, besides the resorptive activity, may have an anabolic effect on bone formation. Zhao et al. reported that the cell surface molecule ephrinB2 present on the osteoclasts mediated anabolic signals to the osteoblasts [32]. In further support of the role of osteoclast in bone formation, Karsdal et al. showed that ostoeclasts secreted non-bone derived factors which induce preosteoblasts to form bone-like nodules [33]. Thereby, these findings indicate the importance of the presence of osteoclasts for induction of bone formation. Better understanding of how osteoclasts respond to different implant surfaces may help contribute to the development of implants that improve osseointergration.

6. Jepson N, Allen F, Moynihan P, Kelly P, Thomason M. Patient satisfaction following restoration of shortened mandibular dental arches in a randomized controlled trial. Int J Prosthodont. 2003;16:409–414.
7. Wolfart S, Heydecke G, Luthardt RG, Marré B, Freesmeyer WB, Stark H *et al.* Effects of prosthetic treatment for shortened dental arches on oral health-related quality of life, self-reports of pain and jaw disability: results from the pilot-phase of a randomized multicenter trial. J Oral Rehabil. 2005; 32:815–822.
8. Thomason JM, Moynihan PJ, Steen N, Jepson NJ. Time to survival for the restoration of the shortened lower dental arch. J Dent Res. 2007;86:646–650.
9. Witter DJ, van Elteren P, Käyser AF, van Rossum MJ. The effect of removable partial dentures on the oral function in shortened dental arches. J Oral Rehabil. 1989;16:27–33.
10. Witter DJ, Van Elteren P, Käyser AF, Van Rossum GM. Oral comfort in shortened dental arches. J Oral Rehabil. 1990;17:137–143.
11. Kuboki T, Okamoto S, Suzuki H, Kanyama M, Arakawa H, Sonoyama W *et al.* Quality of life assessment of bone-anchored fixed partial denture patients with unilateral mandibular distal-extension edentulism. J Prosthet Dent. 1999; 82:182–187.
12. Armellini DB, Heydecke G, Witter DJ, Creugers NH. Effect of removable partial dentures on oral health-related quality of life in subjects with shortened dental arches: a 2-center cross-sectional study. Int J Prosthodont. 2008;21:524–530.
13. Aras K, Hasanreisoğlu U, Shinogaya T. Masticatory performance, maximum occlusal force, and occlusal contact area in patients with bilaterally missing molars and distal extension removable partial dentures. Int J Prosthodont. 2009;22:204–209.
14. Elias AC, Sheiham A. The relationship between satisfaction with mouth and number and position of teeth. J Oral Rehabil. 1998;25:649–661.
15. Witter DJ, Allen PF, Wilson NH, Käyser AF. Dentists'attitudes to the shortened dental arch concept. J Oral Rehabil. 1997;24:143–147.
16. Allen PF, Witter DF, Wilson NH, Käyser AF. Shortened dental arch therapy: views of consultants in restorative dentistry in the United Kingdom. J Oral Rehabil. 1996;23:481–485.
17. Allen PF, Witter DJ, Wilson NH. A survey of the attitudes of members of the European Prosthodontic Association towards the shortened dental arch concept. Eur J Prosthodont Restor Dent. 1998;6:165–169.
18. Fujimaki N, Fueki K, Igarashi Y. A questionnaire study of Japanese dentists' perceptions of risks for overeruption of molars without antagonists and attitude on prosthetic intervention. Prosthodont Res Pract. 2007;6:246–252.
19. Igarashi Y, Ono J, Komiyama Y, Yamashita S. Evaluation to the concept of shortened dental arch; indication and limitation for clinical application. J Jpn Prosthodont Soc. 2003; 47:41–42.
20. Igarashi Y, Arai Y, Hattori Y, Fueki K, Yamashita S. Evaluation to the concept of shortened dental arch 2; assessment by the multi-sectional scientific research. J Jpn Prosthodont Soc. 2003;47:38–40.
21. Baba K, Igarashi Y, Nishiyama A, John MT, Akagawa Y, Ikebe K *et al.* The relationship between missing occlusal units and oral health-related quality of life in patients with shortened dental arches. Int J Prosthodont. 2008;21:72–74.
22. Baba K, Igarashi Y, Nishiyama A, John MT, Akagawa Y, Ikebe K *et al.* Patterns of missing occlusal units and oral health-related quality of life in SDA patients. J Oral Rehabil. 2008;35:621–628.
23. Sugiura T, Fueki K, Igarashi Y. Comparisons between a mixing ability test and masticatory performance tests using a brittle or an elastic test food. J Oral Rehabil. 2009;36:159–167.
24. Kapur KK; Participants of CSP No.86. Veterans Administration Cooperative Dental Implant Study–comparisons between fixed partial dentures supported by blade-vent implants and removable partial dentures. Part I: methodology and comparisons between treatment groups at baseline. J Prosthet Dent. 1987;58:499–512.
25. Sarita PT, Witter DJ, Kreulen CM, Van't Hof MA, Creugers NH. Chewing ability of subjects with shortened dental arches. Community Dent Oral Epidemiol. 2003;31:328–334.
26. van der Bilt A. Human oral function: a review. Braz J Oral Sci. 2002;1:7–18.
27. Zitzmann NU, Hagmann E, Weiger R. What is the prevalence of various types of prosthetic dental restorations in Europe? Clin Oral Implants Res. 2007;18:20–33.

Correspondence: Kenji Fueki, Section of Removable Partial Denture Prosthodontics, Graduate School, Tokyo Medical and Dental University, 1-5-45 Yushima, Bunkyo-ku, Tokyo 113-8549, Japan.
E-mail: kunfu.rpro@tmd.ac.jp

Implantation of green tea catechin α-tricalcium phosphate combination enhances bone repair in rat skull defects

Reena Rodriguez,[1,2] Hisamoto Kondo,[3] Myat Nyan,[1,2] Jia Hao,[1,2] Takayuki Miyahara,[1] Keiichi Ohya,[4] Shohei Kasugai[1,2]

[1]Oral Implantology and Regenerative Dental Medicine, Tokyo Medical and Dental University, Bunkyo-ku, Tokyo 113-8549, Japan
[2]Center of Excellence Program, International Research Center in Molecular Science in Tooth and Bone Diseases, Tokyo Medical and Dental University, Bunkyo-ku, Tokyo 113-8549, Japan
[3]Faculty of Dentistry, Oral Implantology, Iwate Medical University, Morioka, Iwate 020-8505, Japan
[4]Section of Pharmacology, Department of Hard Tissue Engineering, Tokyo Medical and Dental University, Tokyo, Japan

Received 20 July 2010; revised 29 October 2010; accepted 26 November 2010
Published online 17 May 2011 in Wiley Online Library (wileyonlinelibrary.com). DOI: 10.1002/jbm.b.31848

Abstract: The purpose of the present study is to investigate effects of the combination of epigallocatechin-3-gallate (EGCG) and α-tricalcium phosphate (α-TCP) on bone regenerative capacity in a bilateral rat calvarial bone defect model. Materials and methods: Bilateral 5-mm-diameter calvarial defects were created in adult male Wistar rats and filled with preparations of EGCG (0, 0.1, 0.2, 0.4 mg) combined with α-TCP particles. This was done by dissolving EGCG in 100% ethanol (50 μL/14 mg) and dropping under sterile condition. The control group was left unfilled ($n = 8$). The animals were sacrificed at 2 and 4 weeks. Radiological images were taken, and histological analysis was done. Six animals from control (0 mg EGCG + α-TCP) group and (0.2 mg EGCG+ α-TCP) group were labeled with fluorescent dyes and histomorphometrically analyzed ($n = 6$) at 2 and 4 weeks. Results: Histomorphometric analysis revealed that the combination of EGCG and α-TCP at doses of 0.1 and 0.2 mg yielded significantly more new bone formation than untreated control group at 2 and 4 weeks ($p < 0.05$). Mineral apposition rate at 0.2-TCP group was enhanced compared with the one of the positive control α-TCP group at 4 weeks ($p < 0.05$). Conclusion: The combination of α-TCP particles and 0.2 mg EGCG stimulates maximum bone regeneration in rat calvarial defects, and this combination would be potentially effective as bone graft material. © 2011 Wiley Periodicals, Inc. J Biomed Mater Res Part B: Appl Biomater 98B: 263–271, 2011.

Key Words: green tea, epigallocatechin-3-gallate, α-TCP, rat calvarial bone defect, bone formation

INTRODUCTION

Osteoporosis is a skeletal disease characterized by low bone mass and microarchitectural deterioration of bone tissue with a consequent increase in bone fragility and susceptibility to fracture.[1]Recent research suggests that green tea aids in optimizing bone health.[2–4] Epigallocatechin-3-gallate (EGCG), the most abundant and biologically active catechin in green tea, has anti-inflammatory and anticancer properties, the ability to reduce serum lipid and blood pressure and to modulate immune response.[1,5] Additionally, EGCG was found to induce apoptotic cell death of osteoclast-like multinucleated cells[6,7] and ameliorated experimentally induced arthritis in mice.[8] Such pharmacological effects of catechins may be useful for prophylaxis or treatment of inflammatory bone disease. Recent *in vitro* studies show that EGCG increases bone mineral nodules in cell lines.[9,10] However, there has been no study that investigates the effect of the bone regenerative capacity of EGCG *in vivo*.

On the other hand, alpha-tricalcium phosphate (α-TCP) is bioactive and degradable material, which is potentially useful as a bone substitute.[9–11] We have demonstrated that optimum degradation rate and its capacity for space maintenance in addition to its osteoconductive properties make α-TCP an ideal scaffold for bone regeneration.[10,11] Thus, the objective of this study is to investigate whether the combination of EGCG and α-TCP would promote bone regeneration in a rat calvarial defect model.

MATERIALS AND METHODS

Preparation of α-TCP and EGCG combination

α-TCP particles (diameter of 500–710 μm) were kindly supplied from Advance Co. (Tokyo, Japan). α-TCP particles and EGCG (Tokyo Chemical Industry Co.) were combined in the following manner. The latter was dissolved in 100% ethanol, and the solution was dropped onto the α-TCP particles under sterile conditions at a concentration of 50 uL/14 mg and completely dried out in a sterile hood. Uniform

Correspondence to: R. Rodriguez; e-mail: drreenajoseph@gmail.com
Contract grant sponsors: Global Center of Excellence Program, International Research Center for Molecular Science in Tooth and Bone Diseases, Tokyo Medical and Dental University, Tokyo, Japan

distribution of the EGCG into the material was achieved because of the porous nature of the α-TCP particles. Most likely maximum amounts entered through the porosities leaving only minimal amount on the surface of the particles.

α-TCP particles containing the following doses of EGCG were prepared: 0, 0.1, 0.2, and 0.4 mg per 14 mg α-TCP particles. The selection of this range of concentration was based on our previous pilot study. The loading efficacy was determined by dividing the released amount of EGCG by the initial loaded EGCG concentration multiplied by 100%.

EGCG release from α-TCP

The release of EGCG was measured using a UV-Visible spectrophotometer, Nanodrop, ND-1000 (Nanodrop Technologies, Wilmington, USA). The absorbance was measured at 238 nm, and working curve for calculation of EGCG concentrations was established from the absorbance values of six EGCG standard solutions. The samples were placed in 500 uL of 0.1*M* tris buffer solution (pH 7.4) and positioned in an Taitec Personal 11 Shaker (Taitec Corp., Tokyo, Japan) set at 100 rpm and 37°C. The amount of EGCG released into the solution was measured 24 hr after the initial immersion, then every day for 14 days. The percentage of released EGCG at each time point was finally calculated.

Surgical procedures

This study was approved by the institutional committee for animal experiments. Fifty eight adult Wistar rats (18-weeks old) were used. The animals were anesthetized with a combination of ketamine-xylazine (40 and 5mg/kg). The dorsal aspect of the cranium was shaved and prepared aseptically for surgery. A 20-mm-long incision on the scalp was made along the sagittal suture. Skin, subcutaneous tissue, and periosteum were reflected to expose the parietal bones. Two full-thickness bone defects of 5-mm diameter were created in the dorsal part of the parietal bone lateral to the sagittal suture.

A 5-mm trephine bur was used to create the defects. To prevent overheating of the bone edges, copious irrigation with saline was done. Care was taken during the surgical procedure to prevent damage to duramater, which was achieved in all the defects by intermittent drilling technique. After TCP particles were filled in the defects, the periosteum was carefully repositioned and sutured so that TCP particles were stabilized in the defects by pressure from periosteum. In 14 animals, both defects were left untreated to serve as negative control. In 44 animals, both defects were filled with 14 mg of a-TCP or a-TCP combined with 0.1-, 0.2-, or 0.4-mg EGCG, designated as TCP-0, TCP-0.1,TCP-0.2, or TCP-0.4 group, respectively ($n = 8$ for each group). The periosteum and subcutaneous tissues were sutured in place using 4-0 Vicryl polygalactin suture (Ethicon, NJ) and the scalp with 4-0 silk (ELP Akiyma Co., Tokyo, Japan). For bone histomorphometrical analysis, 18 animals were injected with calcein (0.03 g/100 g body weight) and tetracycline (0.09 g/100 g body weight) intraperitoneally, 7 days and 1 day before sacrifice, respectively. Thus, three animals of each of control, TCP-0, TCP-0.2 group ($n = 6$) in 2-week and 4-week groups were fluorescently labeled.

Tissue harvest and radiological analyses

Animals were sacrificed 2 and 4 weeks after surgery. The skin was dissected, and the defect sites along with surrounding bone and soft tissue were removed. Then, X-ray imaging was performed by a micro-CT scanner (InspeXio; Shimadzu Science East Corporation, Tokyo, Japan) with a voxel size of 50 μm/pixel. Tri/3D-Bon software (RATOC System Engineering Co., Tokyo, Japan) was used to make a 3D reconstruction from the obtained set of scans.

Histological evaluation

After the radiological analyses, the specimens were fixed in 10% neutralized formalin for 1 week. The specimens from the animals that had not received vital labeling were decalcified in 5% formic acid for 2 weeks and then embedded in paraffin. Before embedding the samples, an incision was made through the middle of the bone defects to ensure that the microtome sections were made in the area of interest. Coronal sections of 5-μm thickness were prepared, stained with hematoxylin-eosin, and observed under an optical microscope. The values of total defect area and area of newly formed bone were measured with imageJ software, and the bone fill percentage (%) to the total defect was calculated.

Measurement of mineral apposition rate

After harvesting and fixation procedures, the specimens were dehydrated in graded alcohol (60, 70, 80, 90, and100% ethanol), stained with Villanueva Bone stain solution for 2 weeks, and embedded in polyester resin Rigolac (Rigolac-70F, Rigolac-2004, Nisshin EM Co., Tokyo, Japan) resin. Five-micrometer-thick sections were cut coronally (exakt, Mesmer, Ost Einbeck, Germany), and the sections were observed under a fluorescent microscope for fluorochrome labeling. The smallest interlabel distance was measured per dose interval.

Statistical analysis

Data were first analyzed by one-way ANOVA. When this analysis suggested a significant difference between groups ($p < 0.05$), the data were further analyzed by Sheffe post hoc multiple comparison tests.

RESULTS

In vitro release behavior of EGCG from α-TCP

The observed drug loading efficiency of α-TCP for EGCG was 91.45+/−4.74. Approximately 40% of adsorbed EGCG was released after 24 hr. This initial burst release was followed by the gradual and stable release of the drug that was maintained until 2 weeks (Figure 1).

Macroscopic observation

All animals recovered well after surgery. Infection of the wounds was not noted visually. Side effects such as paralysis, convulsions, respiratory distress, or signs of pain were

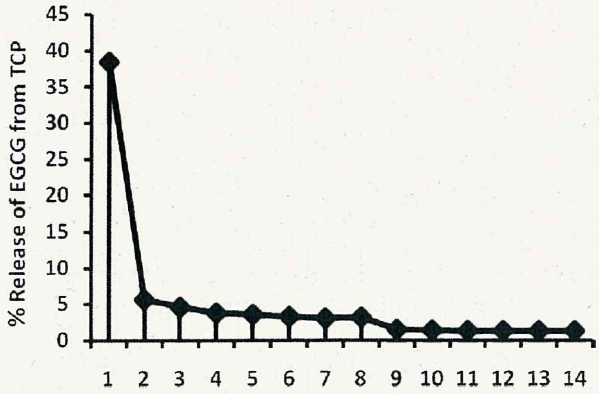

FIGURE 1. *In vitro* release pattern of EGCG from alpha-TCP.

not observed. In all animals, the soft tissue wounds healed uneventfully without showing clinical signs of inflammation expect the one, which is usually observed after the surgery.

Radiological observation

Control group. Scanty amount of new bone was formed in some areas along the margin of bone defect at 2 and 4 weeks [Figure 2(Ia,IIa)].

TCP-0 and TCP-0.4 groups. Scanty amount of bone was formed in between the TCP particles at 2 weeks, which progressively increased at 4 weeks. Compared with the control group, much new bone formation was seen at the defect margins at both 2 and 4 weeks [Figure 2(Ib,e,IIb,e)].

TCP-0.1 and TCP-0.2 groups. At 2 weeks, the new bone was formed not only at the margin of the defect but also in between the α-TCP particles invading the α-TCP particles [Figure 2(Ic,d)]. New bone continued to form between the defect margin and the α-TCP particles at 4 weeks [Figure 2(IIc,d)].

Histological observation

In the control group, at 2 weeks, only a thin layer of new bone was seen at the defect margins without achieving complete defect closure. The central portion of defect was filled with compressed fibrous connective tissue [Figures 4(a) and 5(a)]. More new bone became evident at 4 weeks with bone forming in the middle in most of the defects [Figure 6(a)].

At 2 weeks, only a few areas of new bone formation was seen at the defect margins and between some adjacent α-TCP particles in TCP-0 and TCP-0.4 groups [Figure 3(b,e)]. Each particle demonstrated many spaces inside it forming a reticulate structure. The areas of new bone became increased at 4 weeks [Figure 4(b,e)]. At 2 weeks, there were many areas of new bone in between the α-TCP particles in the TCP-0.2 and TCP-0.1 group, characterized by irregular trabeculae of immature bone and osteoid rimmed by osteoblasts. The new bone seemed to be formed abundantly near

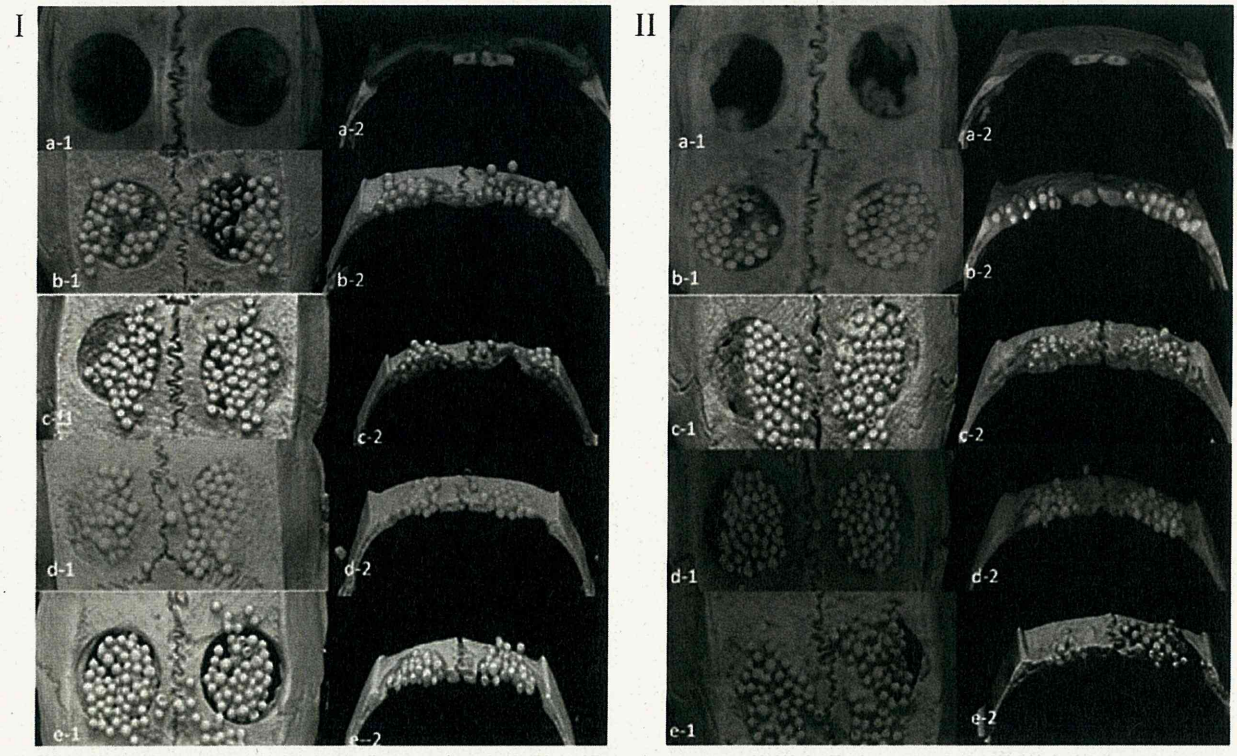

FIGURE 2. Micro-CT images of calvarial defect at I-2w, II-4w representing middle of the bone defect of (a1,a2) control, (b1,b2) TCP, (c1,c2) 0.1-mg EGCG-TCP, (d1,d2) 0.2-mg EGCG-TCP, and (e1,e2) 0.4-mg EGCG-TCP.

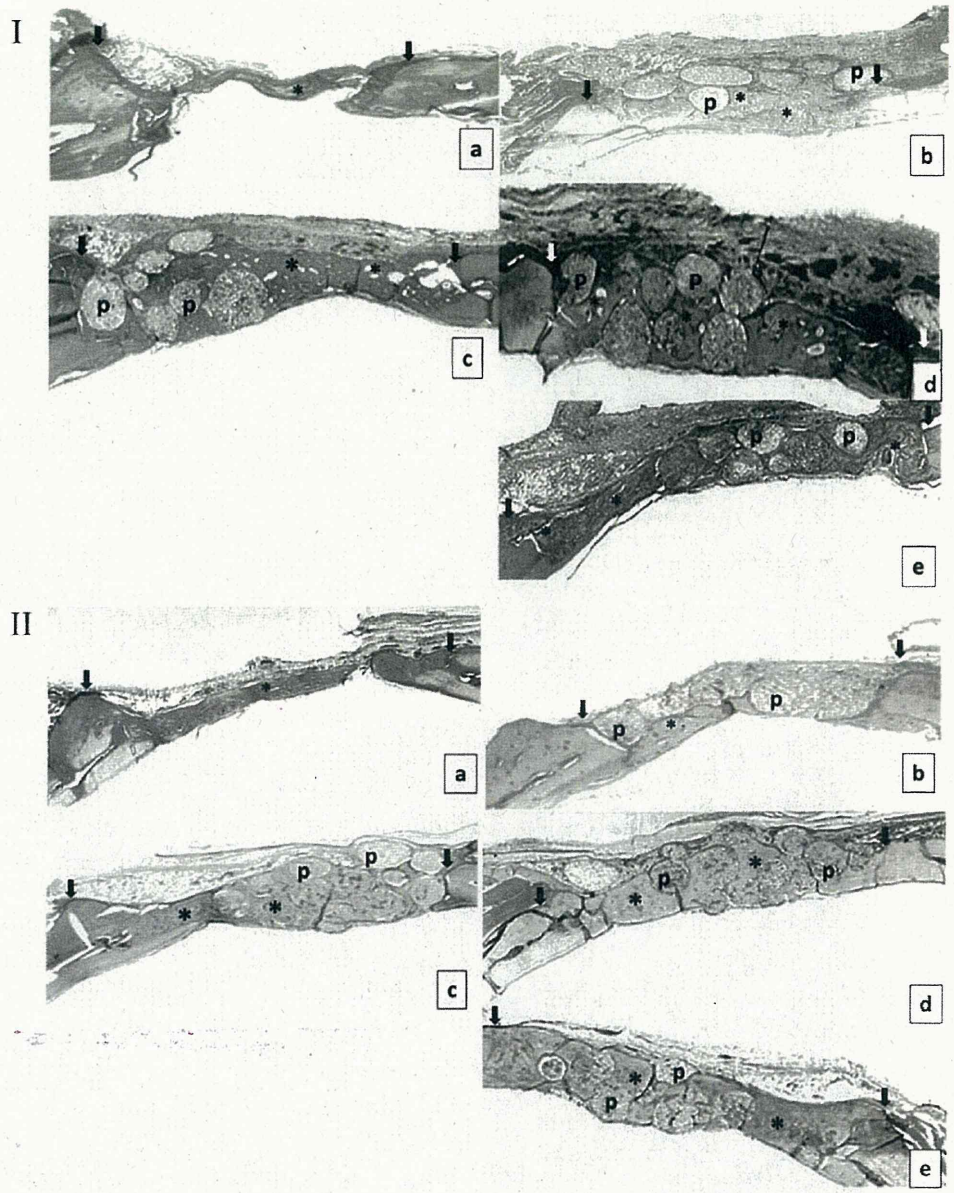

FIGURE 3. Photomicrographs of the calvarial defects at I-2w, II-4w representing middle of the bone defects of (a) control, (b) TCP, (c) 0.1-mg EGCG-TCP, (d) 0.2-mg EGCG-TCP, and (e) 0.4-mg EGCG-TCP. Arrow shows defect margins, * = newly formed bone, and P = TCP particles.

the duramater as well as the defect margin surface. Numerous blood vessels were also associated with the newly formed bone. Active osteoblasts lined around the surface of the α-TCP particles, and bone matrix appeared to be deposited inside the TCP particles [Figure 4(d)]. Thus, the latter appeared to be partially obliterated by bone. At 4 weeks, more advanced bone formation was seen in all the groups [Figure 6(d)]. In TCP-0.4 group, showed many α-TCP particles, which were still invaded by fibroblasts [Figure 5(f)].

Measurement of mineral apposition rate

Mineral apposition rate (MAR) values are shown in Figure 6.

At 2 weeks, there was no statistical difference between control, TCP-0, and TCP-0.2. However, at 4 weeks, the MAR in TCP-0.2 group was significantly higher than those of the control and other TCP groups. Relatively higher apposition rate in the TCP-0.2 group at 4 weeks was in line with the increasing new bone formation in this group at 4 weeks. In all the groups, MARs at 2 weeks were high compared with those at 4 weeks [Figure 6(a,b)].

DISCUSSION

Green tea is prepared by rapidly steaming the fresh leaves of the plant Camellia sinensis to stop the enzymatic

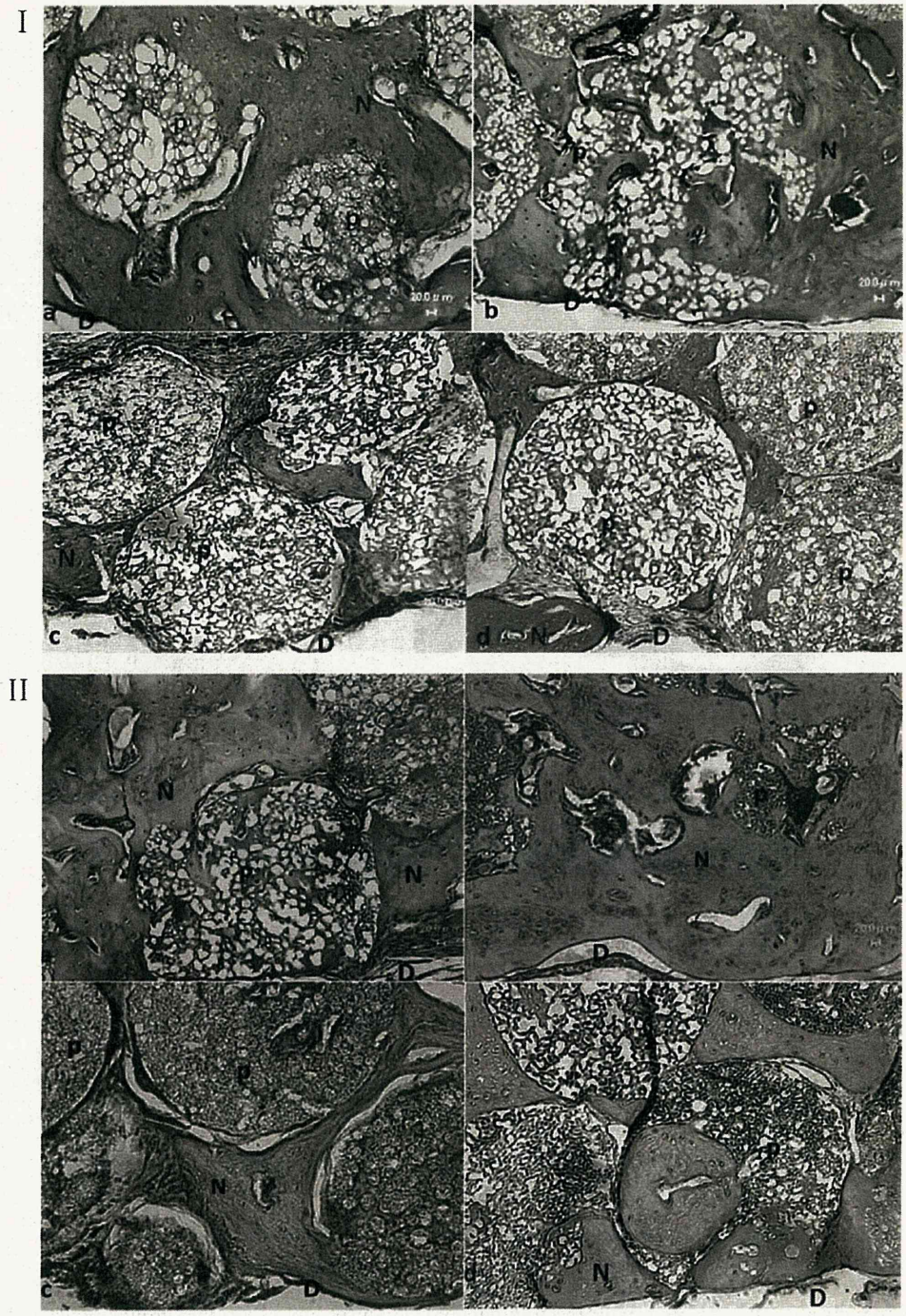

FIGURE 4. Photomicrographs of the calvarial defects at I-2w, II-4w representing middle of the bone defects of (a) 0.1-mg EGCG-TCP, (b) 0.2-mg EGCG-TCP, (c) 0.4-mg EGCG-TCP, and (d) TCP. D = duramater, P = alpha TCP particles, and N = newly formed bone. (Hematoxylin and eosin stain, original magnification ×20, scale bar 20 μm.)

reaction, thus preventing fermentation and generating a catechin-rich stable compound. Epidemiological studies show that habitual consumers of green tea have lesser incidence of osteoporosis-induced hip bone fracture and a higher bone mineral density.[3,4] EGCG, the major component of green tea, is subject of intense investigation, because accumulating chemical and biochemical evidences have shown it to be the most biologically active. EGCG has been reported

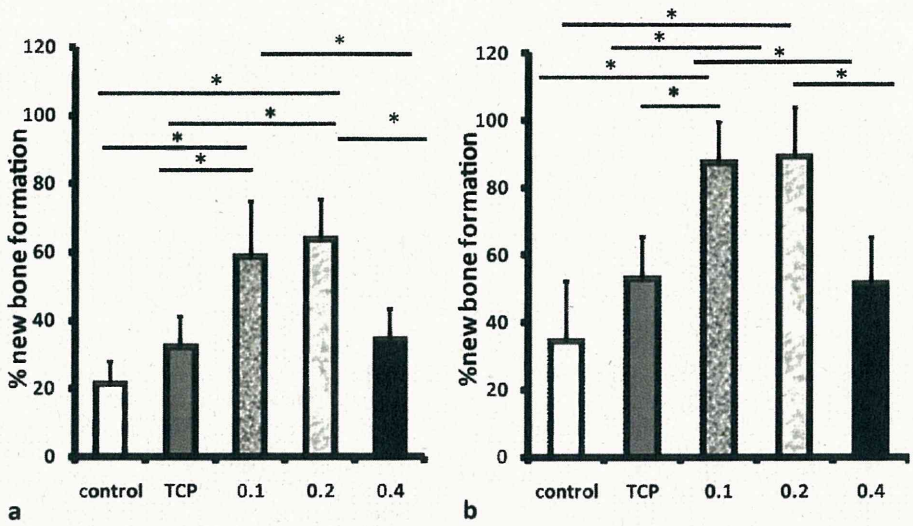

FIGURE 5. Bone volume in the defect at (a) 2 weeks and (b) 4 weeks. Bone volume was measured. Bars and error bars represent means and SEM, respectively. $n = 8$ in all the groups. ANOVA 2 weeks (F4, 35.22.07, $p < 0.0001$), 4 weeks (F4, 35.22.532, $p < 0.0001$.)

to have antioxidant, anti-inflammatory,[5] and anticarcinogenic properties.[12–23] Recently vasodilatory, antiviral, and antimicrobial activities have also been reported.[1,24–26]

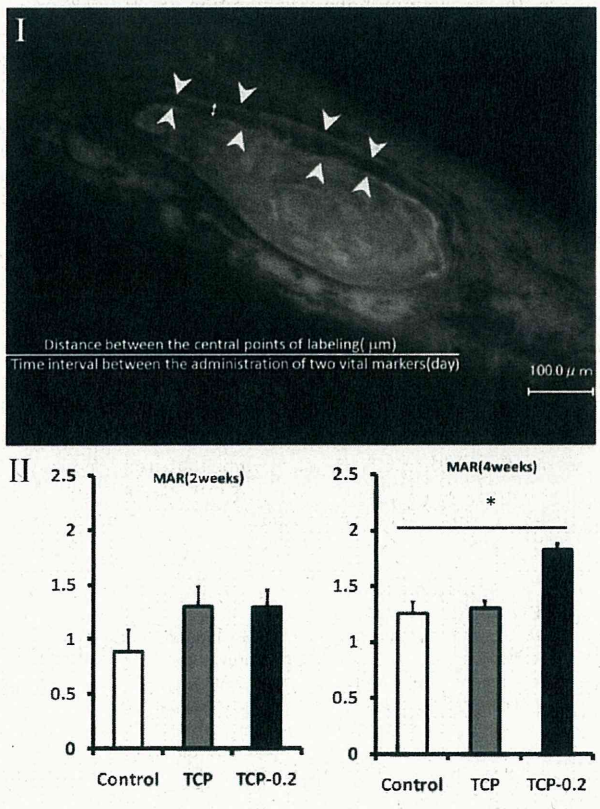

FIGURE 6. (I) Method of measurement of mineral apposition rate; arrow head represent fluorochrome labeling, and double arrow shows the smallest interdistance between the fluorochrome labels. (II) Mineral apposition rates at (a) 2 weeks and (b) 4 weeks (μm/day). Bars and error bars represent means and SEM, respectively. ($n = 6$) for each group at each time point.

Although the possible mechanisms of effects of EGCG on various cells and tissues have been reported, there are only few studies exploring the effects on bone. Recent *in vitro* studies suggest a possible role of EGCG in enhancing bone formation.[6,27,28] Thus, the present study was conducted to test whether local application of EGCG would enhance bone formation *in vivo*. Different doses of EGCG were combined with osteoconductive α-TCP particles and applied to the rat calvarial bone defect model, and it was found that 0.2-mg EGCG induced maximum bone regeneration.

Bone healing takes place as a consequence of a well-orchestrated sequence of molecular signals in the required cells. In addition, creation of a favorable environment with osteoconductive scaffold facilitates the process of bone regeneration. α-TCP is osteoconductive and biodegradable material. The optimal degradation rate and space maintenance capacity attribute to its efficacy in bone regeneration. In our previous study, a combination of α-TCP and simvastatin was found to induce new bone formation.[10,11] Hence, the EGCG and α-TCP combination was applied to test the efficacy in promoting bone regeneration *in vivo*.

Five-millimeter calvarial defect is not critical sized defects, because the defect in untreated control group was bridged with newly formed bone in the present study although regenerated bone in the control group was thin. Since this bone defect model has been widely used,[10,11,29–31] we also used this model in the present study. Notably, bone regeneration in calvarial defect model occurs in unloaded condition. Thus, the results in the present study would be potentially different from bone regeneration of loaded bone.

In the present study, α-TCP worked as scaffold for bone regeneration, and it also released EGCG as a carrier. The results of the release experiment showed biphasic release pattern of EGCG from α-TCP with an initial fast release followed by a slower continuous phase. Although

the exactly similar release pattern of EGCG is not expected *in vivo*, the basic pattern of EGCG release, initial burst release followed by the slow release, would also occur *in vivo*. Bone formation in the bone defect was affected by the dose of EGCG applied to the defect. In our experiment 0.2-mg EGCG consistently showed the highest bone formation.

In the histological sections at 2 weeks, many active osteoblasts were observed bordering around the surface of α-TCP particles and depositing bone matrix. Bone marrow mesenchymal stem cells give rise to osteoprogenitor cells which in turn differentiate to osteoblasts when stimulated. Previous *in vitro* studies showed that EGCG promotes osteoblastic differentiation in mesenchymal D1 cells.[27] Furthermore, significantly higher values of bone volume at 4 weeks in TCP-0.2 group suggested a maximum stimulation of the local cells by EGCG. Significantly increased MARs in this group further suggests the increased activity of individual osteoblasts.

Interestingly, the addition of EGCG was beneficial in promoting new bone formation in the TCP-0.1 and TCP-0.2 groups. However, significantly enhanced bone formation compared with the 0-TCP was not observed in the 0.4-TCP group. This was consistently observed in both the time points. Many health benefits of green tea are primarily attributed to its antioxidant and free radical scavenging ability.[32] Free Radicals are species containing one or more unpaired electrons, such as nitric oxide ($NO^{\bullet -}$). The oxygen radical superoxide ($O_2^{\bullet -}$) and the nonradical hydrogen peroxide (H_2O_2) are produced during normal metabolism. Reactive oxygen species (ROS) have been implicated in many chronic disease states, such as osteoporosis, in inflammatory bone diseases, and during the normal inflammatory phase of healing.[33] It is known that oxidative stress, which occurs due to an excessive amount of reactive oxygen specie, leads to an increase in osteoblast and osteocyte apoptosis, among other changes, and a decrease in osteoblast numbers and the rate of bone formation via Wnt/β-catenin signaling.[34,35] Recent studies showed that oxidative stress inhibited osteoblastic differentiation[35–37] via extracellular signal-regulated kinases (ERKs) and ERK-dependent NF-κB signaling pathways.[38] Osteoblasts can produce antioxidants, such as glutathione peroxidase, to protect against ROS,[35,39] as well as transforming growth factor β(TGF-β), which is involved in a reduction of bone resorption.[40] ROS are also involved in bone resorption with a direct contribution of osteoclast-generated superoxide to bone degradation,[41,42] and oxidative stress increases differentiation and function of osteoclasts.[43] Thus, excessive amount of ROS is potentially harmful to the cell. However, moderately elevated level of ROS is effective in promoting healing by upregulating growth factors and promoting angiogenesis.[2,44]

EGCG is also known to undergo biological transformation and hence has differential effects in response to the concentration and oxygen tension.[2,45–48]

Recent review of literature suggests that the bioactive components in green tea positively influences bone health by four different mechanisms[35,49]: decreased oxidative stress,[50] increased activity of antioxidant enzymes,[51–55] decreased expression of proinflammatory mediators,[2,56,57–60] and a possible osteoimmunological action.[2,35,56]

EGCG modulates the level of reactive oxygen and nitrogen species which in turn dose dependently signals for a repair response, while it also inhibits proliferation and/or induces apoptosis.[2,56] Since these effects are dose-dependent, it is reasonable that EGCG stimulated bone regeneration at the optimal dose but not stimulated it at the higher dose in the present study.

In the present study, we demonstrated that an optimal concentration of EGCG was critical for eliciting the signal for bone formation. Although the mechanism of the stimulative effect of EGCG and α-TCP combination in the present study is unclear, we speculate it as the following. The biphasic release pattern from α-TCP particles may have provided optimal amount of EGCG during the initial inflammatory phase of healing, which was effective in down regulating the overall inflammatory response. The antioxidant property may have reduced the acute inflammatory phase and elicited a quicker reparative phase in wound healing. In addition, the osteoconductivity and space maintenance capacity of α-TCP particles may also have played an important role in the maximum bone regeneration in TCP-0.2 group by providing a suitable niche for cellular proliferation. More bone was consistently found in all the particle-filled defects compared with the empty control defects. The space-maintaining capacity of α-TCP was thus advantageous in the outcome of bone augmentation procedure. The empty unfilled defects, which served as the negative control group, revealed only a thin layer of new bone formation along the periphery of defect.

CONCLUSION

This study demonstrated the bone promoting effect of local application of EGCG. It was determined that 0.2 mg was the optimal dose for the maximum bone regeneration of 5-mm-diameter bone defects in rat calvaria when applied in combination with α-TCP. Further studies are required to validate the effect of this optimal dose of EGCG with α-TCP combination in different clinical conditions.

REFERENCES

1. Tosetti F, Noonan D, Albini A. Metabolic regulation and redox activity as mechanisms for angioprevention by dietary phytochemicals. Int J Cancer 2009;125:1997–2003.
2. Nakagawa H, Wachi M, Woo JT, Kato M, Kasai S, Takahashi F, Lee IS, Nagai K. Fenton reaction is primarily involved in a mechanism of (-)-epigallocatechin-3-gallate to induce osteoclastic cell death. Biochem Biophys Res Commun 2002;292:94–101.
3. Wu C, Yang Y, Yao W, Lu F, Wu J, Chang C. Epidemiological evidence of increased bone mineral density in habitual tea drinkers. Arch Intern Med 2002;162:1001–1006.
4. Hegarty V, May H, Khaw K. Tea drinking and bone mineral density in older women. Am J Clin Nutr 2000;71:1003–1007.
5. Rahman I, Biswas S, Kirkham P. Regulation of inflammation and redox signaling by dietary polyphenols. Biochem Pharmacol 2006;72:1439–1452.

6. Lin RW, Chen CH, Wang YH, Ho ML, Hung SH, Chen IS, Wang GJ. (-)-Epigallocatechin gallate inhibition of osteoclastic differentiation via NF-kappaB. Biochem Biophys Res Commun 2009; 379:1033–1037.
7. Lee J, Jin H, Shim H, Kim H, Ha H, Lee Z. Epigallocatechin-3-gallate inhibits osteoclastogenesis by down-regulating c-Fos expression and suppressing the nuclear factor-kappaB signal. Mol Pharmacol 2010;77:17–25.
8. Morinobu A, Biao W, Tanaka S, Horiuchi M, Jun L, Tsuji G, Sakai Y, Kurosaka M, Kumagai S. (-)-Epigallocatechin-3-gallate suppresses osteoclast differentiation and ameliorates experimental arthritis in mice. Arthritis Rheum 2008;58:2012–2018.
9. Kamitakahara M, Ohtsuki C, Miyazaki T. Review paper: Behavior of ceramic biomaterials derived from tricalcium phosphate in physiological condition. J Biomater Appl 2008;23:197–212.
10. Kihara H, Shiota M, Yamashita Y, Kasugai S. Biodegradation process of alpha-TCP particles and new bone formation in a rabbit cranial defect model. J Biomed Mater Res B Appl Biomater 2006; 79:284–291.
11. Nyan M, Sato D, Kihara H, Machida T, Ohya K, Kasugai S. Effects of the combination with alpha-tricalcium phosphate and simvastatin on bone regeneration. Clin Oral Implants Res 2009;20: 280–287.
12. Boehm K, Borrelli F, Ernst E, Habacher G, Hung SK, Milazzo S, Horneber M. Green tea (Camellia sinensis) for the prevention of cancer. Cochrane Database Syst Rev 2009:CD005004.
13. Butt M, Sultan M. Green tea: Nature's defense against malignancies. Crit Rev Food Sci Nutr 2009;49:463–473.
14. Chen L, Zhang H. Cancer preventive mechanisms of the green tea polyphenol (-)-epigallocatechin-3-gallate. Molecules 2007;12: 946–957.
15. Chen D, Milacic V, Chen MS, Wan SB, Lam WH, Huo C, Landis-Piwowar KR, Cui QC, Wali A, Chan TH, Dou QP. Tea polyphenols, their biological effects and potential molecular targets. Histol Histopathol 2008;23:487–496.
16. Clement Y. Can green tea do that? A literature review of the clinical evidence. Prev Med 2009;49:83–87.
17. Johnson J, Bailey H, Mukhtar H. Green tea polyphenols for prostate cancer chemoprevention: A translational perspective. Phytomedicine 2010;17:3–13.
18. Khan N, Mukhtar H. Multitargeted therapy of cancer by green tea polyphenols. Cancer Lett 2008;269:269–280.
19. Lambert J, Yang C. Mechanisms of cancer prevention by tea constituents. J Nutr 2003;133:3262S–3267S.
20. Lin J, Liang Y. Cancer chemoprevention by tea polyphenols. Proc Natl Sci Counc Repub China B 2000;24:1–13.
21. Lin J. Cancer chemoprevention by tea polyphenols through modulating signal transduction pathways. Arch Pharm Res 2002;25: 561–571.
22. Nagle D, Ferreira D, Zhou Y. Epigallocatechin-3-gallate (EGCG): chemical and biomedical perspectives. Phytochemistry 2006;67: 1849–1855.
23. Neergheen V, Bahorun T, Taylor E, Jen L, Aruoma O. Targeting specific cell signaling transduction pathways by dietary and medicinal plant bioactive compounds in cancer chemoprevention. Toxicology 2010;5;278:229–241.
24. Schneider C, Segre T. Green tea: Potential health benefits. Am Fam Physician 2009;79:591–594.
25. Shimizu M, Weinstein I. Modulation of signal transduction by tea catechins and related phytochemicals. Mutat Res 2005;591: 147–160.
26. Shimizu M, Shirakami Y, Moriwaki H. Targeting receptor tyrosine kinases for chemoprevention by green tea catechin, EGCG. Int J Mol Sci 2008;9:1034–1049.
27. Chen C, Ho M, Chang J, Hung S, Wang G. Green tea catechin enhances osteogenesis in a bone marrow mesenchymal stem cell line. Osteoporos Int 2005;16:2039–2045.
28. Vali B, Rao L, El-Sohemy A. Epigallocatechin-3-gallate increases the formation of mineralized bone nodules by human osteoblast-like cells. J Nutr Biochem 2007;18:341–347.
29. Freeman E, Turnbull RS. The value of osseous coagulum as a graft material. J Periodontal Res 1973;8:229–236.
30. Bosch C, Melsen B, Vagervik K. Guided bone regeneration in calvarial bone defects using polytetrafluroethelene membranes. Cleft palate craniofac J 1995;32:311–317.
31. Nyan M, Miyahara T, Noritake K, Hao J, Rodriguez R, Kuroda S, Kasugai S. Molecular and tissue responses in the healing of rat calvarial defects after local application of simvastatin combined with alpha tricalcium phosphate. J Biomed Mater Res Part B: Appl Biomater 2010;93B:65–73.
32. Rahman I, Biswas SK, Kirkham PA. Regulation of inflammation and redox signaling by dietary polyphenols. Biochem Pharmacol 2006;72:1439–1452.
33. Frantz S, Bauersachs J, Ertl G. Post-infarct remodelling: Contribution of wound healing and inflammation. Cardiovasc Res 2009;81: 474–481.
34. Manolagas SC. Scavenging H2O2while making cholesterol. Endocrinology 2008;149:3264–3266.
35. Shen CL, Wang P, Guerrieri J, Yeh J, Wang JS. Protective effect of green tea polyphenols on bone loss in middle-aged female rats. Osteoporosis Int 2008;19:979–990.
36. Mody N, Parhami F, Saraflan TA, Demer LL. Oxidative stress modulates osteoblastic differentiation of vascular and bone cells. Free Radic Biol Med 2001;31:509–519.
37. Fatokun AA, Stone TW, Smith RA. Responses of differentiated MC3T3-E1 osteoblast-like cells to reactive oxygen species. Eur J Pharmacol 2008;587:35–41.
38. Bai XC, Lu D, Bai J, Zheng H, Ke ZY, Li XM, Luo SQ. Oxidative stress inhibits osteoblastic differentiation of bone cells by ERK and NF-κB. Biochem Biophys Res Commun 2004;314:197–207.
39. Dreher I, Schütze N, Baur A, Hesse K, Schneider D, Köhrle J, Jakob F. Selenoproteins are expressed in fetal human osteoblast-like cells. Biochem Biophys Res Commun 1998;245:101–107.
40. Fuller K, Lean JM, Bayley KE, Wani MR, Chambers TJ. A role for TGF-β in osteoclast differentiation and survival. J Cell Sci 2000; 113:2445–2453.
41. Yang S, Madyastha P, Bingel S, Ries W, Key L. A new superoxide generating oxidase in murine osteoclasts. J Biol Chem 2001;276: 5452–5458.
42. Sontakke AN, Tare RS. A duality in the roles of reactive oxygen species with respect to bone metabolism. Clin Chim Acta 2002; 318:145–148.
43. Garrett JR, Boyce BF, Oreffo RO, Bonewald L, Poser J, Mundy GR. Oxygen-derived free radicals stimulate osteoclastic bone resorption in rodent bone in vitro and in vivo. J Clin Invest 1990; 85:632–639.
44. Gordillo G, Sen C. Revisiting the essential role of oxygen in wound healing. Am J Surg 2003;186:259–263.
45. Choi Y, Jeong Y, Lee Y, Kwon H, Kang Y. (-)Epigallocatechin gallate and quercetin enhance survival signaling in response to oxidant-induced human endothelial apoptosis. J Nutr 2005;135: 707–713.
46. Hou Z, Lambert J, Chin K, Yang C. Effects of tea polyphenols on signal transduction pathways related to cancer chemoprevention. Mutat Res 2004;555:3–19.
47. Sugisawa A, Umegaki K. Physiological concentrations of (-)-epigallocatechin-3-O-gallate (EGCg) prevent chromosomal damage induced by reactive oxygen species in WIL2-NS cells. J Nutr 2002; 132:1836–1839.
48. Ramos S. Effects of dietary flavonoids on apoptotic pathways related to cancer chemoprevention. J Nutr Biochem 2007;18: 427–442.
49. Shen C-L, Yeh JK, Cao JJ, Wang J-S. Green tea and bone metabolism. Nutr Res 2009;29:437–456.
50. Weisburger JH. Tea and health: The underlying mechanisms. Proc Soc Exp Biol Med 1999;220:271–275 [Review].
51. Romas E, Gillespie MT, Martin TG. Involvement of receptor activator of NF-κB ligand and tumor necrosis factor-alpha in bone destruction in rheumatoid arthritis. Bone 2002;30:340–346.
52. Miyaura C, Inada M, Matsumoto C, Ohshiba T, Uozumi N, Shimizu T, Ito A. An essential role of cytosolic phospholipase A2alpha in prostaglandin E2-mediated bone resorption associated with inflammation. J Exp Med 2003;197:1303–1310.
53. Tatakis DN. Interleukin-1 and bone metabolism: A review. J Periodontol 1993;64:416–431.

54. Johnson RA, Boyce BF, Mundy GR, Roodman GD. Tumoros producing human tumor necrosis factor induced hypercalcemia and osteoclastic bone resorption in nude mice. Endocrinology 1989;124:1424–1427.
55. Wallach S, Avioli LV, Feinblatt JD, Carstens JH Jr. Cytokines and bone metabolism. Calcif Tissue Int 1993;53:293–296.
56. Virgili F, Marino M. Regulation of cellular signals from nutritional molecules: A specific role for phytochemicals, beyond antioxidant activity. Free Radic Biol Med 2008;45:1205–1216.
57. Blair HC, Athanasou NA. Recent advances in osteoclast biology and pathological bone resorption. Histol Histopathol 2004;19: 189–199.
58. Kwan Tat S, Padrines M, Théoleyre S, Heymann D, Fortun Y. IL-6, RANKL, TNF-alpha/IL-1: Interrelations in bone resorption pathophysiology. Cytokine Growth Factor Rev 2004;15:49–60 [Review].
59. Robinson LJ, Borysenko CW, Blair HC. Tumor necrosis factor family receptors regulating bone turnover: New observations in osteoblastic and osteoclastic cell lines. Ann N Y Acad Sci 2007; 1116:432–443.
60. Moreland LW, Curtis JR. Systemic nonarticular manifestations of rheumatoid arthritis: Focus on inflammatory mechanisms. Semin Arthritis Rheum 2009;39:2.

Int. J. Oral Maxillofac. Surg. 2011; 40: 200–206
doi:10.1016/j.ijom.2010.10.002, available online at http://www.sciencedirect.com

International Journal of
Oral & Maxillofacial Surgery

Research Paper
Imaging Technology

Biomechanical effect of crestal bone osteoplasty before implant placement: a three-dimensional finite element analysis

M. Hudieb[1,2], S. Kasugai[1,2]
[1]Department of Oral Implantology and Regenerative Dental Medicine, Division of Oral Health Sciences, Graduate School, Tokyo Medical and Dental University, Japan; [2]Global Center of Excellence Program, International Research Center for Molecular Science in Tooth and Bone Diseases, Tokyo Medical and Dental University, Japan

M. Hudieb, S. Kasugai: Biomechanical effect of crestal bone osteoplasty before implant placement: a three-dimensional finite element analysis. Int. J. Oral Maxillofac. Surg. 2011; 40: 200–206.

Abstract. This study investigated the biomechanical effects of crestal bone osteoplasty and flattening procedures carried out in edentulous knife-edge ridges to restore bone width before implant placement on the virtually placed implants using finite element methods. Three-dimensional models representing a knife-edged alveolar bone with two different crestal cortical bone thicknesses (1.6 mm, thin group; 3.2 mm, thick group) were created. Gradual crestal bone osteoplasty with 0.5 mm height intervals was simulated. Cylindrical implants with abutments and crowns were constructed and subjected to oblique loads. Maximum stress was observed at the cervical region around the implant neck. Different osteoplasty levels showed different stress values and distributions. Highest compressive stress was observed in the flat models (60.8 MPa and 98.3 MPa in thick and thin groups, respectively), lowest values were observed when osteoplasty was limited to the sharp edge (36.8 MPa and 38.9 MPa in thick and thin groups, respectively). The results suggested that eliminating the sharp configuration in knife-edge ridges improved stress and strain outcomes, but flattening the alveolar crest and/or uncovering the cancellous bone resulted in a marked increase in compressive stress and strain values in the peri-implant bone that may influence the longevity of implants placed in these ridges.

Keywords: osteoplasty; dental implant; knife edge ridge; bone stress; strain; finite element analysis.

Accepted for publication 5 October 2010
Available online 4 December 2010

Dental implants have been widely used for prosthetic rehabilitation of partially and completely edentulous patients. Adequate available bone dimensions are considered a prerequisite for successful and predictable implant treatment[1–3]. Following tooth extraction, continuous bone resorption usually takes place and results, initially, in a narrow ridge with a knife-edge form[4–7].

A relatively large percentage of narrow ridges with knife-edge configuration have been reported at the edentulous mandibular and maxillary bony crests[21]. Treatment for completely removable dentures may require preprosthetic surgical reduction of the sharp edges to prevent painful denture pressure points at the knife-edged borders. Increasing the horizontal width of the bone prior to implant placement is required in these ridges to host the implant in the alveolar bone properly[16,21]. This can be achieved by osteoplasty, performed to eliminate and flatten the thin sharp edge configuration, and/or additional bone augmentation and surgical procedures such as onlay bone grafts[5], guided bone regeneration[3] horizontal distraction[25] and

0901-5027/020200+07 S36.00/0

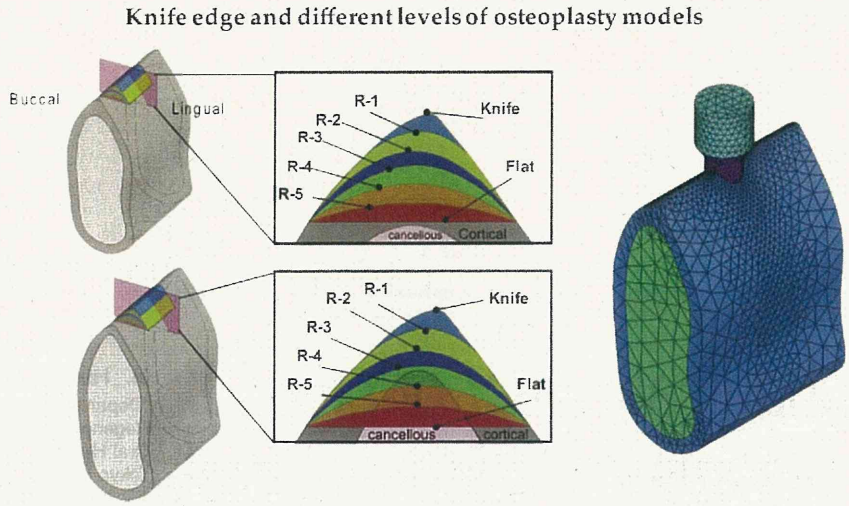

Fig. 1. Basic mandibular bone segments used for the thin and thick cortical bone groups. Simulation of flattening and several levels of osteoplasty in the middle part of the bone segment are shown in the cross-sectional image. The name of each model refers to the outer bone curvature used. Cancellous bone was exposed in R4, R5 and Flat models of the thin cortical bone group. The meshed FE model of the thick knife edge bone is shown on the right.

sagittal osteotomies of the edentulous ridge[5].

When the narrow width is limited to the alveolar bone crest in ridges with adequate height, osteoplasty or flattening procedures are recommended rather than bone augmentation procedures[16]. The local anatomy and geometry of the peri-implant bone influence the distribution and intensity of the stresses generated in the surrounding bone, because of the mechanical interlocking relationship between the implant and the surrounding bone[10,19]. Excessive stresses generated around dental implants are considered to be one of the main causes of peri-implant bone loss and/or implant failure[6,12].

The effect of crestal bone osteoplasty and the flattening procedures that precede implant placement on the biomechanical behavior of dental implants has not been assessed in relation to the stress and strain generated around the dental implants that will be placed in these ridges. The purpose of this study was to evaluate the biomechanical effect of surgical reduction and flattening of the narrow alveolar bone crest on the biomechanical behavior of the future implants using three dimensional (3D) finite element analysis (FEA). Several methods have been used to evaluate the biomechanical aspect of dental implants such as FEA, strain gauges and photo-elastic models. Of these methods, FEA is considered the method of choice to calculate the stresses generated in complex geometries and to evaluate different variables simultaneously[9].

Materials and methods

Model design

A 3D model of an edentulous mandibular segment with knife-edge configuration was constructed. A cross-sectional CT scan for the mandibular first premolar region was selected with a bucco-lingual dimension of less than 2 mm at the alveolar crest level, which is considered as the knife-edge ridge according to Pietrokovski et al.[21].

The image was plotted and used to determine x and y coordinates for points that describe the outline of the external cortical bone surface. These coordinates were imported into the FEM software (ANSYS 9.0, ANSYS Inc., PA, USA) as keypoints that were connected by smooth lines/curves using a 'spline algorithm'. The area was divided into a cancellous core surrounded by a layer of cortical bone. Two basic bone models (Knife models) were created with exactly the same external cortical bone outline, but different cortical bone thicknesses at the crestal region. The first had a uniform layer of cortical bone 1.6 mm thick (thin group), and the second had cortical bone thickness at the crestal region of 3.2 mm (thick group). The two-dimensional images were extruded in the z axis to create a 3D bone model with a mesio-distal length of 20 mm. The alveolar bone models were approximately 12.25 mm wide bucco-lingually and 28.5 mm heigh infero-superiorly.

Flattening and several levels of osteoplasty were simulated for the two basic Knife alveolar bone models by gradually subtracting the bone in the crestal region until a flattened surface was obtained in the Flat models, with 1 mm of bone on the buccal and distal sides. A vertical distance of 0.5 mm (measured from the highest point vertically) was removed each time to produce the Reduction models: R1, R2, R3, R4 and R5 (Fig. 1). The reduction was performed in a curved way to preserve the bucco-lingual width and was limited to the central part of the bone segment with a mesio-distal length of 8 mm, corresponding to the standard implant diameter (4 mm) and 2 mm on both mesial and distal sides. 14 models were constructed (Fig. 1). A cylindrical implant, 4 mm in diameter and 10 mm long, was placed vertically in the alveolar ridge, with a simplified abutment and crown, 6 mm in diameter and 8 mm high.

Loading and boundary conditions

All materials were assumed to be isotropic, homogeneous and linearly elastic. The interfaces between the materials were assumed bonded or osseointegrated. Young's moduli of the cortical bone, cancellous bone, implant, and prosthetic structures were assumed to be 15 GPa, 1.5 GPa, 110 GPa and 96.6 GPa, respectively. A Poisson's ratio of 0.3 was used for all the materials, except for the prosthetic structures, which had a ratio of 0.35[9].

The models were fixed in all directions on the mesial and distal surfaces of the bone[23]. A load of 200 N applied 30°

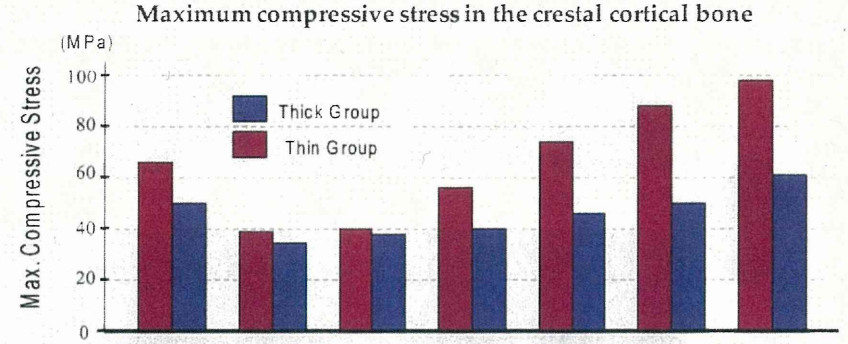

Cortical Bone thickness (mm)	Knife edge	R-1	R-2	R-3	R-4	R-5	Flat
Thick	3.2	2.7	2.2	1.7	1.2	0.7	0.2
Thin	1.6	1.1	0.6	0.1	0.0	0.0	0.0

Fig. 2. Maximum compressive stress values (MPa) in the crestal bone around the necks of the implants on application of the oblique loads: Thin, thin cortical bone group; thick, thick cortical bone group. The thickness of the crestal cortical bone at the midline is shown in each model of the two groups.

buccal from the vertical axis[15] was applied at the center of the occlusal surface of the crown.

All models were meshed with 20-node tetrahedral elements. A convergence test was performed to determine the number of elements to ensure the validity of calculations. A finer mesh was generated around the neck of the implant. Depending on the model, element numbers ranges were 75,175–82,793 and 90,435–98,328 in the thick and thin groups, respectively. The compressive stress and strain results were calculated and recorded for all models in the bone structures.

Results

The maximum compressive stress and strain values in each of the 14 models are summarized in Figs 2 and 3. On loading the implant, maximum compressive stresses were observed at the cervical region of the cortical bone in all models. In the knife-edge models, the maximum stress was noted at the mesial and distal sides of the implant neck on the sharp bone edge (Figs 4 and 5). Maximum cortical bone stress values were 49.5 MPa and 66.3 MPa in the thick and thin models, respectively. A marked reduction in stress was noted when the sharp edge was eliminated in R1 models with peak compressive stress of 36.8 MPa and 38.9 MPa for thick and thin cortical bone models, respectively. The maximum compressive stress was increased progressively as the alveolar crest height became reduced. The highest compressive stress value occurred around the implant in the flat models with 60.8 MPa and 98.3 MPa in the thick and thin cortical bone models, respectively (Figs 4 and 5).

In the cancellous bone, the maximum stress values were considerably lower than those in the cortical bone in all models. Peak stresses were observed at the crestal region under the cortical bone plate around the implant neck in R3, R4, R5 and Flat models of the thin group and the Flat model of the thick group. In the rest of the models, peak stresses were observed at the lingual side of the implant apex (Fig. 6). The distribution of the maximum compressive strain was similar to the compressive stress in the corresponding models.

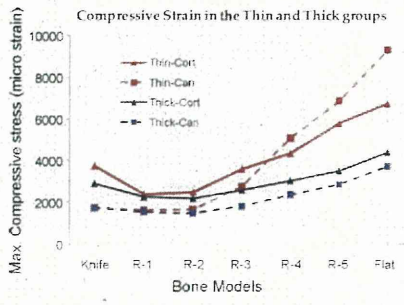

Fig. 3. The maximum compressive strain values (micro strain) in the cortical and cancellous bones in each model of the thin and thick groups. Cort-Thin, cortical bone in the thin group; Canc-Thin, cancellous bone in the thin group; Cort-Thick, cortical bone in the thick group; Canc-thick, cancellous bone in the thick group.

Discussion

FEA is used increasingly to predict the performance of dental implants. It can be undertaken by studying mechanical parameters such as the stress or strain generated in the implant and surrounding bone structures[9]. FEA comprises several steps starting with the pre-processing stage, in which the implant and bone models are developed. To obtain accurate results and precisely evaluate the biomechanical aspects of treatment options, it is essential to develop and design models that represent clinical conditions. Previous FEA studies have tended to ignore the local anatomy of the crestal bone and implant site preparation, for example by representing the alveolar bone with a simplified rectangle in two dimensions or a block with rectangular cross-section in 3D models. When anatomical models are used, the crestal region is often modified to have a flat contour with a uniform cortical bone layer. Recently, more accurate, realistic models have been constructed using CT scan data and other advanced digital imaging techniques. The data used are commonly selected for the ideal bone morphology of a well rounded alveolar bone (class III Cawood and Howell classification[4]) which does not represent other bone morphology types.

Pietrokoviski et al.[21] investigated the characteristics of edentulous ridges in

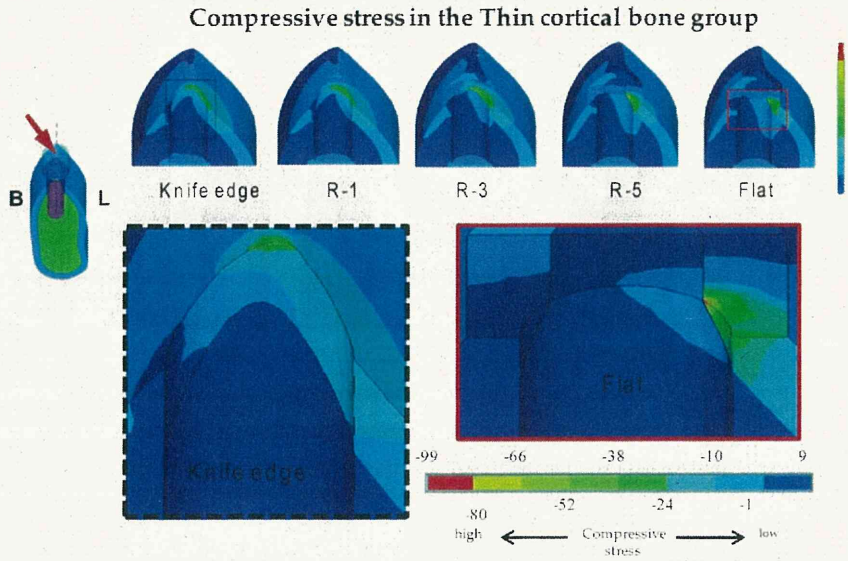

Fig. 4. The effects of gradual reduction of the alveolar bone crest and the exposure of cancellous bone on the compressive stress in the thin cortical bone group. The figure on the left indicates the viewing angle and force direction (red arrow). Models are sectioned halves and viewed from the mesial side (upper graphics). The crestal regions in the Knife-edge and Flat models are enlarged (lower graphics). The same contour scale was used for all models in the thin group. The red area represents the highest compressive stress.

human jaws. They reported 43% with a knife-edge alveolar crest in the mandible and 38% in the premolar region. Osteoplasty procedures in which the alveolar crest is surgically reduced or flattened are considered to be the most common approach that routinely restores the required width for implant placement in thin and/or knife-edge ridges[17]. In this study, bone models represented class IV (knife-edge ridge) and different levels of osteoplasty.

Altering the morphology and geometry of the crestal bone by osteoplasty procedures was found to influence the distribution and magnitude of generated peri-implant bone stress and strain. In the knife-edge models, a relatively high compressive stress was found at the mesial and distal sides of the implant neck, where the sharp, thin edge is located. Lower stress, with an even distribution, was observed at the lingual side. The strong, bony curvature (characterized by the acute angle, measured between the vertical axis of the implant and the external lingual cervical bone surfaces) presented at the lingual side probably accounts for the reduction of stress at this region; when implants are attached to a cortical bone with stronger curvature, stress will be directed from the outer cortical edge to the inner bone[11,24]. As the sharp edge was eliminated in R1 models, the stress generated was redistributed over a larger area. Thus the maximum stress was reduced in

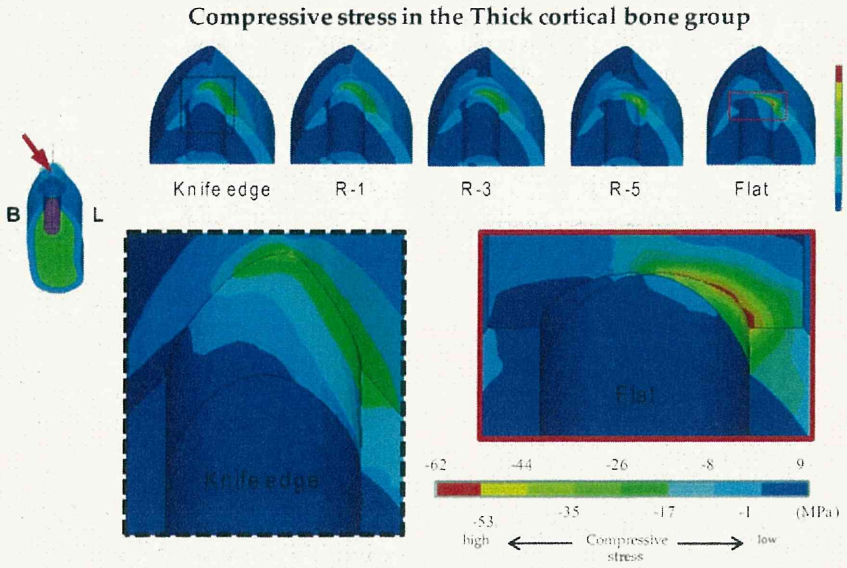

Fig. 5. The effects of gradual reduction of the alveolar bone crest on the compressive stress in the thick cortical bone group. The crestal regions in the Knife-edge and Flat models are enlarged (lower graphics). The same contour scale was used for all models in the thick group.

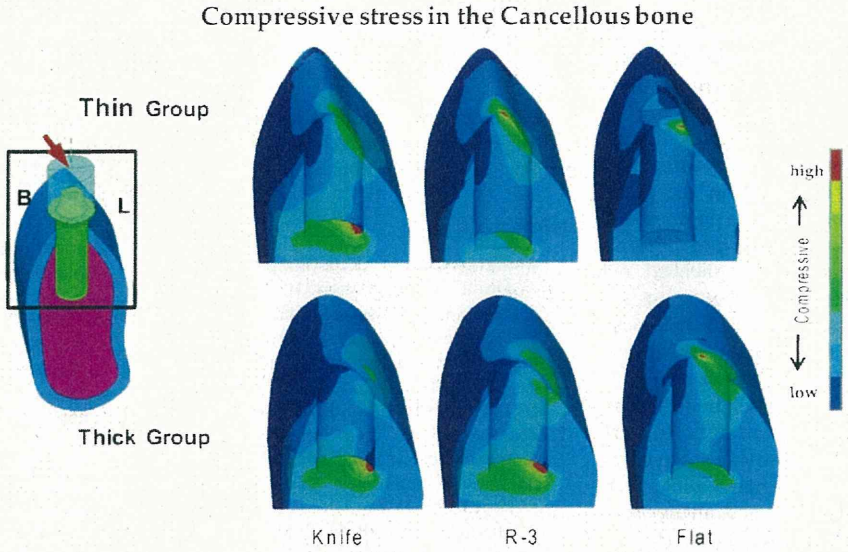

Fig. 6. The compressive stress distributions in the cancellous bone were shown in the Knife edge, R3, and Flat models of the thick (upper graphics) and thin (lower graphics) groups sectioned halves and viewed from the mesial side. Red contour represents the maximum stress in each model. (For interpretation of the references to color in this figure legend, the reader is referred to the web version of the article.)

the mesial and distal regions around the implant. Maintaining the strong curvature lingually in these models (R1) may explain the preservation of the low stress level, which was evenly distributed on the lingual side. A progressive increase of stress was observed in the rest of the models as the curvature strength and the cortical bone thickness were reduced further.

Reduction of crestal bone curvature increased the resultant stress and strain, regardless of the cortical bone thickness. This was confirmed when comparing different bone reduction levels. For instance, the thick R4 model showed a higher maximum stress value than the thin R2 model, although the cortical bone thickness in the former was two times larger than the latter (Fig. 2). This demonstrates the importance of the crestal bone contour as a key factor in the resultant stress outcome around dental implants.

Bone models with larger crestal cortical bone thickness exhibited a relatively lower peri-implant stress and strain compared with the corresponding models with the same osteoplasty reduction levels but with less cortical bone thickness. This agrees with previous reports in the literature[10,20].

When the alveolar crest is surgically reduced or flattened, it may result in sharp edges to the remaining cortical bone and exposure of the cancellous bone. These changes in the bone could lead to local stress and strain concentrations and fatigue failures[8]. This would explain why the maximum stress was located at the sharp cortical edges along with the substantial increase in stress and strain values in the R3, R4, R5 and Flat models in the thin cortical bone group.

The distribution of peak stresses in the cancellous bone was influenced by the presence and the thickness of the cortical bone layer. In bone models with compromised cortical bone thickness (thin R3, and thick Flat) or with uncovered cancellous bone (thin R4, R5 and Flat), maximum stresses were found at the crestal region. This might be due to the inward displacement of the thin cortical bone plate in those models.

Osteoplasty procedures resulted in reduction of the cortical bone support/thickness and/or exposure of the cancellous bone to direct forces in the crestal region. The amount of bone reduction depends on the diameter of the implant to be placed and the width of the available bone. Class IV (knife-edge) has shown a larger need for crestal bone reduction[7]. In this study, an implant with a standard diameter of 4 mm was used to provide the 1 mm of supporting bone at the buccal and lingual sides, the required bucco-lingual width was 6 mm. Depending on the thickness of the cortical bone layer, osteoplasty may result in exposing the cancellous bone as demonstrated in the thin group, which represents the average cortical bone thickness. The crestal cortical bone was doubled in the thick group to study the influence of gradual reduction and flattening with and without cancellous bone exposure.

The potential fatigue damage to the bone is expected to occur under excessive dynamic loading that exceeds 4000 microstrain under compressive forces[8,18]. This is attributed to the accumulation of induced micro-damage that exceeds the bone repair capacity[2,8]. The compressive stress and strain parameters were used as a risk scale in this study but inherent simplifications made in FEA may limit the direct application of quantitative results obtained from these analyses.

The aim of this study was not to predict the exact *in vivo* stresses, but to explore the possible differences that result as a consequence of modifying crestal bone morphology. Limitations of this study include single static loading and the vertical placement of the implant and the bone quality used. Previous studies have indicated that in comparative analysis, the relative accuracy of the results is not affected by these parameters[14]. A cylindrical non-threaded implant was used in this study as it is considered the neutral design[1], and to establish a baseline from which other implant designs can be compared in further studies. The implant–bone attachment was assumed to be perfectly and continuously bonded. This is because of the absence of reliable data regarding the interfacial tensile strength.

In this study, the stress and strain generated around the dental implant were investigated immediately after osseointegration. Accordingly, neither bone resorption nor corticalization was represented. The central region of cancellous bone was

uncovered in some models, but the cortical bone support that is considered critical for implant stability was maintained for implants in all models.

Based on the results of this study, osteoplasty procedures may critically affect the stress and strain outcomes in the peri-implant bone structure. The high stress and strain generated around dental implants could cause mechanical overloading of the bone and may result in alveolar bone loss that affects the long term success of the implant treatment. Exposing the cancellous bone has significantly increased cancellous bone strain around the implant. Accordingly, from a biomechanical point of view, a sharp edge should be carefully eliminated while flattening the crestal region and uncovering cancellous bone should be avoided.

Rounding or reduction of the alveolar bone may redistribute and decrease the stress. Based on the results of this study, and taking into consideration the wide variation in bone morphology and cortical bone thickness among individuals, it may be impossible to draw a definitive conclusion regarding the limit to which the crestal region can be reduced without causing considerable increase in the resultant stresses.

When the alveolar bone ridge is rounded or flattened, the available bone height for implant placement is reduced. Consequently, shorter implants are placed in these ridges[7,17]. Simultaneously, the crown height space is increased. This change in the crown/implant ratio increases the stress generated in the peri-implant bone structures[22]. In the current study, the intrabony implant length and the supra-crestal abutment and prosthesis heights were standardized to exclude the effect of crown/implant ratio.

In conclusion, crestal bone osteoplasty procedures performed prior to implant placement may improve the resultant stress and strain outcomes around the dental implant neck when the sharp edge of the knife-edge ridge is eliminated. Flattening the alveolar crest and uncovering the cancellous bone may have the disadvantage of significantly increasing stress and strain in the crestal bone region.

Funding

None.

Competing interests

None declared.

Ethical approval

Not required.

Acknowledgements. The authors would like to thank Dr. N. Wakabayashi and Prof. T. J. Wright for their helpful comments.

References

1. Abu-Hammad O, Khraisat A, Dar-Odeh N, El-Maaytah M. Effect of dental implant cross-sectional design on cortical bone structure using finite element analysis. Clin Implant Dent Relat Res 2007: **9**: 217–221 doi CID048 [pii] 10.1111/j.1708-8208.2007.00048.x.
2. Brunski JB. In vivo bone response to biomechanical loading at the bone/dental–implant interface. Adv Dent Res 1999: **13**: 99–119.
3. Buser D, Bragger U, Lang NP, Nyman S. Regeneration and enlargement of jaw bone using guided tissue regeneration. Clin Oral Implants Res 1990: **1**: 22–32.
4. Cawood JI, Howell RA. A classification of the edentulous jaws. Int J Oral Maxillofac Surg 1988: **17**: 232–236.
5. Chiapasco M, Romeo E, Vogel G. Tridimensional reconstruction of knife-edge edentulous maxillae by sinus elevation, onlay grafts, and sagittal osteotomy of the anterior maxilla: preliminary surgical and prosthetic results. Int J Oral Maxillofac Implants 1998: **13**: 394–399.
6. Duyck J, Ronold HJ, Van Oosterwyck H, Naert I, Vander Sloten J, Ellingsen JE. The influence of static and dynamic loading on marginal bone reactions around osseointegrated implants: an animal experimental study. Clin Oral Implants Res 2001: **12**: 207–218 doi clr120304 [pii].
7. Eufinger H, Konig S, Eufinger A. The role of alveolar ridge width in dental implantology. Clin Oral Investig 1997: **1**: 169–177.
8. Frost HM. A brief review for orthopedic surgeons: fatigue damage (microdamage) in bone (its determinants and clinical implications). J Orthop Sci 1998: **3**: 272–281.
9. Geng JP, Tan KB, Liu GR. Application of finite element analysis in implant dentistry: a review of the literature. J Prosthet Dent 2001: **85**: 585–598 doi S0022-3913(01)57431-4 [pii] 10.1067/mpr.2001.115251.
10. Holmes DC, Loftus JT. Influence of bone quality on stress distribution for endosseous implants. J Oral Implantol 1997: **23**: 104–111.
11. Hylander WL. Mandibular function and biomechanichal stress and scaling. Am Zool 1985: **25**: 223–240.
12. Kim Y, Oh TJ, Misch CE, Wang HL. Occlusal considerations in implant therapy: clinical guidelines with biomechanical rationale. Clin Oral Implants Res 2005: **16**: 26–35 doi CLR1067 [pii]10.1111/j.1600-0501.2004.01067.x.
13. Lekholm U, Adell R, Lindhe J, Branemark PI, Eriksson B, Rockler B, Lindvall AM, Yoneyama T. Marginal tissue reactions at osseointegrated titanium fixtures. II. A cross-sectional retrospective study. Int J Oral Maxillofac Surg 1986: **15**: 53–61.
14. Meijer HJ, Starmans FJ, Steen WH, Bosman F. A three-dimensional, finite-element analysis of bone around dental implants in an edentulous human mandible. Arch Oral Biol 1993: **38**: 491–496 doi 0003-9969(93)90185-O [pii].
15. Mericske-Stern R, Assal P, Mericske E, Burgin W. Occlusal force and oral tactile sensibility measured in partially edentulous patients with ITI implants. Int J Oral Maxillofac Implants 1995: **10**: 345–353.
16. Misch CE. Available bone and dental implant treatment plans. In: Misch CE, ed: Contemporary Implant Dentistry. St. Louis: Mosby Elsevier 2008 : 178–194.
17. Misch CE. Divisions of available bone in implant dentistry. Int J Oral Implantol 1990: **7**: 9–17.
18. Mosley JR, Lanyon LE. Strain rate as a controlling influence on adaptive modeling in response to dynamic loading of the ulna in growing male rats. Bone 1998: **23**: 313–318 doi S8756-3282(98)00113-6 [pii].
19. Nagasao T, Kobayashi M, Tsuchiya Y, Kaneko T, Nakajima T. Finite element analysis of the stresses around fixtures in various reconstructed mandibular models – part II (effect of horizontal load). J Craniomaxillofac Surg 2003: **31**: 168–175 doi S1010518203000295 [pii].
20. Petrie CS, Williams JL. Probabilistic analysis of peri-implant strain predictions as influenced by uncertainties in bone properties and occlusal forces. Clin Oral Implants Res 2007: **18**: 611–619 doi CLR1384 [pii] 10.1111/j.1600-0501.2007.01384.x.
21. Pietrokovski J, Starinsky R, Arensburg B, Kaffe I. Morphologic characteristics of bony edentulous jaws. J Prosthodont 2007: **16**: 141–147 doi JOPR165 [pii] 10.1111/j.1532-849X.2007.00165.x.
22. Tada S, Stegaroiu R, Kitamura E, Miyakawa O, Kusakari H. Influence of implant design and bone quality on stress/strain distribution in bone around implants: a 3-dimensional finite element analysis. Int J Oral Maxillofac Implants 2003: **18**: 357–368.
23. Teixeira ER, Sato Y, Akagawa Y, Shindoi N. A comparative evaluation of mandibular finite element models with different lengths and elements for implant biomechanics. J Oral Rehabil 1998: **25**: 299–303.
24. van Eijden TM. Biomechanics of the mandible. Crit Rev Oral Biol Med 2000: **11**: 123–136.
25. Watzak G, Zechner W, Tepper G, Vasak C, Busenlechner D, Bernhart

T. Clinical study of horizontal alveolar distraction with modified micro bone screws and subsequent implant placement. Clin Oral Implants Res 2006: **17**: 723–729 doi CLR1267 [pii] 10.1111/j.1600-0501.2006.01267.x.

Address:
Malik Hudieb
Department of Oral Implantology and Regenerative Dental Medicine
Division of Oral Health Sciences
Graduate School
Tokyo Medical and Dental University
1-5-45 Yushima
Bunkyo
Tokyo 113-8549
Japan
Tel.: +81 358034664
fax: +81 358034664.
E-mail: mhudeab@gmail.com

次世代の歯科再生治療の実現に向けて

大島正充 Masamitsu Oshima [1)]
辻　　孝 Takashi Tsuji [1~3)]
1）東京理科大学　総合研究機構
2）東京理科大学大学院　基礎工学研究科生物工学専攻
3）株式会社オーガンテクノロジーズ

歯科再生治療の実現に向けたこれまでの取り組み

次世代の歯科治療として，「歯科再生治療」が期待されている[1)]．歯科再生治療には，歯髄や歯周組織を幹細胞やサイトカインにより治療する組織再生治療に加え，疾患や傷害により喪失した歯を再生により取り戻す，歯の再生治療の技術開発が進められている[2)]．歯をまるごと再生するための戦略として，歯の器官原基である歯胚を再生し，胎児期の発生プログラムを再現することにより再生歯を発生させる技術開発が進められている[1,3~5)]．

歯をまるごと再生する治療技術を開発するには，三次元的な細胞操作により歯胚を再生する技術を開発し，再生歯胚を歯の喪失部位に移植をして萌出，機能させる再生治療や，歯胚に由来する歯の組織をすべて再生した再生歯ユニットを作製し，口腔内に移植，生着させる治療方法が考えられる（図1）．

まず筆者らは，2007年に，未分化な上皮細胞と間葉細胞を高細胞密度で区画化して器官原基を再生する三次元的な細胞操作技術である「器官原基法」を開発し，正常な組織構造を有する歯や毛包を高頻度に再生することを可能とし，幅広い器官再生の研究に道を拓いた（図2）[6)]．さらにこの技術を応用することにより，歯の太さと咬頭数の制御も可能とした[7)]．

次に筆者らは，再生歯胚移植による歯の再生のコンセプトの実証に向け，研究を行った（図1）．成体マウスの歯の喪失部位に再生歯胚を移植すると，再生歯胚は正常に発生し，再生歯が口腔内に萌出して咬合するとともに，機械的外力に応答する歯根膜機能や，侵害刺激を中枢へ伝達可能な神経機能を有する機能的に完全な歯を再生可能であることを明らかとした（図3）[8)]．

再生歯ユニット移植による機能的な歯の再生

歯の再生治療のもう1つのコンセプトとして，再生歯胚から発生可能な歯の組織を再生することにより，成熟した再生歯と歯根膜，歯槽骨を有する再生歯ユニットを作製し，歯の喪失部位に移植して生着させる方法が考えられる（図1）．

この治療方法は，インプラント治療と同じように，移植後，即時あるいは早期の機能回復が期待される．このコンセプトは歯の再生だけではなく，即時機能可能な段階にまで発生させた再生器官を移植して，即時に機能不全状態を回復させることができれば，生命に関わる臓器の再生にも適応可能な治療技術として発展する可能性を有している[9)]．